Proceedings of the Twenty-ninth (2019) International Ocean and Polar Engineering Conference **www.isope.org**
Honolulu, Hawaii, USA, June 16-21, 2019

ISBN 978-1 880653 85-2; ISSN 1098-6189

Parametric Vibration of Top-tensioned Risers with Internal Flow

Fajun Yu[1,2], Binqi Xie[1,2], Han Wu[1,2,3], Qi Wang[1,2], Hemu Shi[1,2], Xiaohui Zeng[1,2]*
[1] Key Laboratory for Mechanics in Fluid Solid Coupling Systems, Institute of Mechanics, Chinese Academy of Sciences
Beijing, China
[2]School of Engineering Science, University of Chinese Academy of Sciences
Beijing, China
[3]State Key Laboratory of Hydraulic Engineering Simulation and Safety, School of Civil Engineering, Tianjin University.
Tianjin, China

ABSTRACT

This paper studies the effects of internal fluid on the stability of parametric vibration of a top-tensioned riser (TTR), where the effects of internal flow on the parametric instability charts are analyzed. Results show that both the internal flow density (mass per unit length) and velocity exert an influence on the instability charts. The internal flow density has more influence on the instability region. As the internal flow density changes, both the shape and the position of the instability charts will change.

KEY WORDS: top-tensioned riser; TTR; parametric vibration; internal flow; instability analysis; Hill equation.

INTRODUCTION

As the offshore oil and gas industry moves into deeper waters, where the difficulty of the exploration of oil and gas increases dramatically, it puts forward higher requirement for deep-water production equipment. As a key equipment linking the floater and subsea production system, the vibration characteristics of a top-tensioned riser (TTR) become a popular issue in engineering design. In the marine environment, a TTR is subjected to various loads including top floater motion, internal fluid, sea current and so on. Due to the large slenderness ratio, the riser may undergo large motions under the actions of adverse loads, even though a certain tension is applied at the top end of the riser. Therefore, it is essential to explore the vibration response analysis of the riser.

The parametric vibration of a TTR will occur in the horizontal direction due to the effects of the platform's heave motions, which will lead to the destruction of risers. Parametric resonance of marine cable was propose and analyzed for the first time by Hsu (1975), where the effects of the velocity square damping of the fluid to decrease the amplitude growth in unstable case are studied. Based on using a direct solution approach to solve the differential equations, Chung and Whitney (1981) studied the heave induced dynamic loads on an 18,000-Ft ocean mining pipe. And then they investigated the effect of axial deformation to deep-ocean pipe and found that it is significant to dynamic behavior of the low flexible riser (Chung et al. 1994*a*; Chung et al. 1994*b*). Patel and Park (1995) examined the combination of the forcing and parametric excitation for tethers of tensioned buoyant platforms, in different water depths. By using a numerical method, Chatjigeorgiou and Mavrakos (2002) researched vertical the non-linear dynamic response of marine risers, which are subjected to parametric excitation due to motions of marine structure. And then, effects of damping on riser stability for risers subjected to parametric excitation have been studied by their subsequent works (Chatjigeorgiou 2004; Chatjigeorgiou and Mavrakos, 2005). Based upon using finite element method, Park and Jung (2002) investigated the response of risers under combined parametric and forcing excitations. In their numerical works, the relative amplitudes of this kind of combination to an isolated forcing excitation for various water depths, environmental conditions and vessel motions are considered. Chandrasekaran et al. (2006) studied the dynamic response of tethers and TLPs, assuming that tension varies along the tether length. Aiming at deep-water risers, Brugmans (2005) compared the difference of the parametric vibration instability of three boundary models in detail, and developed simple formulae to predict platform heaving frequency corresponding to different instability regions p under parametric excitation of riser system. By using Floquet theory, Kuiper et al. (2008) investigated riser instability under parametric excitation and obtained instability mechanisms of two kinds of parametric vibrations. The first is induced by periodic time variation of the axial tensions. The another one is due to large motions of the platform. Xu et al. (2008) investigated the hill instability of TLP tethers by considering the coupled motion of surge and heave of TLPs. And then, they study parametric instability of long slender marine structures by using the Lyapunov-Poincareper method, the modified Lyapunov-Poincareper method and the harmonic balance method (Xu et al., 2011). Chung (2010) presented the full-scale measurements for 5,000-m-long hanging pipe and the theoretical prediction of its end's dynamic behavior. Fujiwara et al. (2011) studied the response of riser Vortex-Induced Vibration under parametric excitation using experiment methods. By using a multi-frequency excitation, Yang et al. (2013) gave a prediction for the parametric instability of TTRs under the action of irregular waves. A frequency domain method was proposed by Lei et al. (2014) to investigate the

effect of the parametric excitation on the frequency domain responses of the riser. Under combined forcing excitation and parametric excitation, a coupled dynamic analysis of a marine riser is investigated by Wang et al. (2015). A vertical linear model to simulate the dynamic tension force is also used in their work. Zhang and Tang (2015) studied the parametric instability analysis of TTRs considering the linearly varying tension along the length. The governing equation is solved by using the Galerkin method. Lei et al. (2017) applied extended precise integration method (EPIM) to research the dynamic instability of deep-water TTRs under the fluctuating axial tension. Li and Chen (2018) studied the parametric vibration instability of a riser by considering the pre-stress. They investigated the influence of complex pre-stress on frequency, mode shapes, and instability characteristics of the parametric vibration for TTR.

The deep-water riser is a marine structure with large slenderness ratio, and the internal flow will have significant effect on the vibration and stability of deep-water riser due to the large slenderness ratio increases. Much recent works have studied the internal flow effect of marine riser conveying flowing fluid (Atadan et al., 1997; Keber and Wiercigroch, 2008; Chatjigeorgiou, 2010). By using the singular perturbation technique, Wu and Lou (1991) researched the effect of the internal flow for the lateral motion of a marine riser. They found that the internal flow can reduce the effect of the top tension. Guo and Lou (2008) investigated the internal flow effect on the Vortex-Induced Vibration of risers. They found that internal flow will aggravate riser vibration. And then, much works focus on research the internal flow Vortex-Induced Vibration of flexible marine risers (Meng and Chen, 2012; Meng et al., 2017a; Meng et al., 2017b). Meng et al. (2018) studied the effects of centrifugal force and Coriolis force on the parametric instability, which are introduced by internal flow in deep-water drilling risers.

These studies add to our understanding of internal flow and riser parametric vibration. Researches on the parametric vibration of risers are mostly limited to the influence of transverse displacement caused by platform heave motion. But for harsh ocean conditions, the platform will produce large surge motions, which will also have unwanted impacts on the parametric vibration of risers. This point was deeply studied by Xu et al. (2008), but they did not consider the internal flow effect. In the current studies, the researches about internal flow effect on risers' vibration are mainly focused on the vortex-induced vibration, while studies about the internal flow density and the internal flow velocity on the parameter vibration of risers is relatively few. The internal flow effect and the coupling of the surge and heave motions of the top platform are simultaneously taken into account in the present paper and the axial and transverse coupled vibration equations of the TTR are established. Due to the axial nonlinear resonance response will not be excited in general, the axial motion can be ignored and only the transverse motion of the riser is considered. The transverse motion equation is further degraded to the nonlinear Hill equation describing the parametric vibration of the riser. The paper mainly studies the effect of internal flow density (mass per unit length) and internal flow velocity on the parametric instability of a TTR, respectively.

The structure of this paper is as follows. Some related formula derivation is listed in§2, where the governing equation of transverse vibration of the TTR is derived in §2.1 and the derivation of instability regions of the nonlinear Hill equation considering the internal flow parameters (including internal flow density and internal flow velocity) is listed in §2.2. In §3, we discussed the effect of internal flow on instability regions, where the effect of internal flow velocity is discussed in §3.1 and the effect of internal flow density is discussed in §3.2. §4 is the conclusion.

FORMULATION

Mathematical Calculation Model

In general, the combined axial and transverse vibration of the TTR is such significant due to its large slenderness ratio, thus, the vibration of the TTR can be analyzed by using the nonlinear vibration theory of beam. Based on using the nonlinear vibration analysis theory of pipe conveying fluid of Paidoussis (1998), the governing equation is obtained. To simplify the analysis, we consider the riser as an Euler–Bernoulli beam simply supported at both ends and only its axial vibrations and transverse vibrations perpendicular to the current direction are considered. Fig. 1(a) is the structure and vibration schematic diagram of a TTR, where a Cartesian coordinate system is established and its origin is at the bottom of the riser. The positive ox axis is located on the axis of the riser and points vertically upwards. L is the length of the riser, $u(x, t)$ the axial displacement of the riser, $w(x, t)$ the transverse displacement of the riser, $h(t)$ the displacement of platform heave motion and $y(t)$ the displacement of platform surge motion.

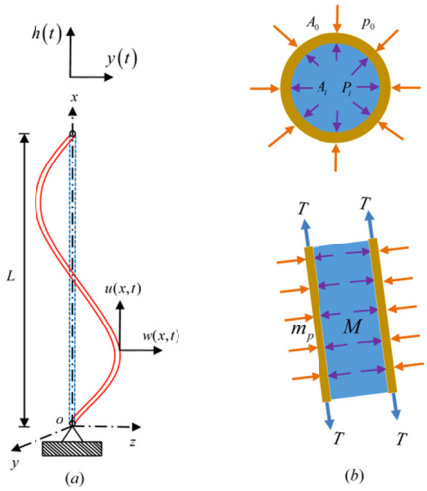

Fig. 1 Schematic diagram of vibration and stress of the TTR.

Under the action of internal pressure, external pressure, and the external force, the cross-sectional area of riser will have great change, which will affect the internal flow velocity. Fig. 1(b) is schematic diagram of radial and axial section stress of the TTR, where p_i is the internal pressure, p_0 the external pressure, A_i the area of the inner diameter and A_0 the area of the external diameter. Hence the cross-sectional area of riser can be defined as $A = A_0 - A_i$. m_p and M are mass per unit length of riser wall and internal flow density (mass per unit length of internal flow), respectively. T is the tension exerted by the platform on the riser, U_0 the internal flow velocity for static riser. Assuming that the state of the riser is from completely free of load to multiple loads of axial force and internal and external pressure, the internal area of riser changes to A_i', which can be written as

$$A_i' = A_i\left\{1+\frac{1}{E}\left[(1-\mu)\sigma_r - \mu\sigma_z + (1+\mu)\tau\right]\right\}^2, \quad \text{where } r = r_i. \tag{1}$$

Here E and μ are Young's modulus and the Poisson's ratio of riser material. σ_r and σ_z are radial and z-direction stress of the riser, respectively. τ is the shear stress of riser and r_i the inner radius of riser. According to the conservation of flow, the internal flow velocity of vibrating riser after deformation can be obtained

$$U_2 = U_0\left[1-\frac{2}{E}(1+\mu)\frac{A_i}{A_0-A_i}(p_i-p_0)\right.$$
$$\left.-\frac{(2-4\mu)(p_iA_i-p_0A_0)}{EA}+2\mu\varepsilon+2\mu\frac{T}{EA}\right], \tag{2}$$

where

$$\varepsilon_1 = -\frac{2}{E}(1+\mu)\frac{A_i}{A_0-A_i}(p_i-p_0)-\frac{(2-4\mu)(p_iA_i-p_0A_0)}{EA}, \tag{3}$$

$$\varepsilon = \frac{\partial u}{\partial x}+\frac{1}{2}\left(\frac{\partial w}{\partial x}\right)^2. \tag{4}$$

Here ε_1 is the strain caused by internal and external pressure of the riser and ε the strain due to riser deformation.

Based on using the separation body method, coupled equations combined axial and transverse vibrations of a TTR with internal flow are established. Assuming that the length of a certain micro-segment of the riser does not change before and after the riser deformation, as shown in Fig. 2, we discuss a certain micro-segment of the riser. Q_1 is the axial force exerted on the micro-segment, Q_2 the shear force applied to the micro-segment and M_1 the bending moment on the micro-segment.

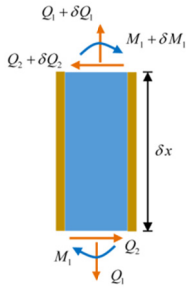

Fig. 2 Schematic diagram of riser micro-segment.

The force balance equation of the micro-segment can be expressed as

$$\frac{\partial(Q_1\cos\theta)}{\partial x}-\frac{\partial(Q_2\sin\theta)}{\partial x}-(M+m_p)g = m_p\frac{\partial^2 u}{\partial t^2}+M\frac{D^2(x+u)}{Dt^2}, \tag{5}$$

$$\frac{\partial(Q_1\sin\theta)}{\partial x}+\frac{\partial(Q_2\cos\theta)}{\partial x} = m_p\frac{\partial^2 w}{\partial t^2}+M\frac{D^2 w}{Dt^2}, \tag{6}$$

where

$$\sin\theta = \frac{\partial w}{\partial x}\left(1-\frac{\partial u}{\partial x}-\frac{1}{2}\left(\frac{\partial w}{\partial x}\right)^2\right), \qquad \cos\theta = 1-\frac{1}{2}\left(\frac{\partial w}{\partial x}\right)^2. \tag{7}$$

Here θ is the angle between x-axis and the axis of the riser and g the gravitational acceleration.

Considering the strain due to pressure of internal and external fluids and the strain caused by axial and transverse vibration of the riser, it gives:

$$Q_1 = T+T_1+EA\varepsilon, \tag{8}$$

$$Q_2 = -\frac{EI}{1+\varepsilon}\frac{\partial^2\theta}{\partial x^2}, \tag{9}$$

where

$$T = T_0+\left[-M\frac{\mathrm{d}U_0}{\mathrm{d}t}-(M+m_p)g+\rho_F A_o g\right](L-x), \tag{10}$$

$$T_1 = (1-2\mu)(\rho_L A_i g-\rho_F A_o g)(L-x), \tag{11}$$

$$\frac{\partial\theta}{\partial x} = \frac{1}{(1+\varepsilon)^2}\left[\frac{\partial^2 w}{\partial x^2}\left(1+\frac{\partial u}{\partial x}\right)-\frac{\partial w}{\partial x}\frac{\partial^2 u}{\partial x^2}\right]. \tag{12}$$

Here T_1 is the axial force variation caused by internal and external fluid pressure, I the polar moment of inertia for riser and T_0 the additional tension. ρ_L and ρ_F are internal and external fluid density respectively. Substituting Eq. (4) and Eqs. (7) ~ (12) into Eqs. (5) and (6), the governing equations for the coupled axial and transverse vibration of the riser can be obtained. Given that the axial natural frequency of the top tension riser is much higher than the excitation frequency of the wave load, the axial nonlinear resonance response will not be excited and then the axial motion can be ignored. Reserved to third order small quantity, the governing equation of transverse vibration of the riser can be expressed as follows:

$$(M+m_p)\frac{\partial^2 w}{\partial t^2}+2MU_0\left(1+\varepsilon_1+2\mu\varepsilon+2\mu\frac{T}{EA}\right)(1-\varepsilon)\frac{\partial^2 w}{\partial t\partial x}$$
$$+MU_0{}^2\left(1+\varepsilon_1+2\mu\varepsilon+2\mu\frac{T}{EA}\right)^2(1-2\varepsilon)\frac{\partial^2 w}{\partial x^2}$$
$$+M\left\{\frac{\mathrm{d}U_0}{\mathrm{d}t}\left(1+\varepsilon_1+2\mu\varepsilon+2\mu\frac{T}{EA}\right)\right.$$
$$\left.+2\mu\left[\frac{\partial^2 u}{\partial x\partial t}+\frac{\partial w}{\partial x}\frac{\partial^2 w}{\partial x\partial t}\right]U_0\right\}(1-\varepsilon)\frac{\partial w}{\partial x}$$
$$+MU_0{}^2\left(1+\varepsilon_1+2\mu\varepsilon+2\mu\frac{T}{EA}\right)\left\{\frac{2}{EA}(1+\mu)A_i(\rho_L g-\rho_F g)\right.$$
$$+\frac{(2-4\mu)(\rho_L A_i g-\rho_F A_o g)}{EA}+2\mu\left(\frac{\partial^2 u}{\partial x^2}+\frac{\partial w}{\partial x}\frac{\partial^2 w}{\partial x^2}\right)$$
$$\left.-2\mu\frac{1}{EA}\left[-M\frac{\mathrm{d}U_0}{\mathrm{d}t}-(M+m_p)g+\rho_F A_o g\right]\right\}(1-\varepsilon)\frac{\partial w}{\partial x}$$
$$-\left\{T_0+\left[-M\frac{\mathrm{d}U_0}{\mathrm{d}t}-(M+m_p)g+\rho_F A_o g\right](L-x_0)\right\}$$
$$\times\left[\frac{\partial^2 w}{\partial x^2}-\frac{\partial^2 u}{\partial x^2}\frac{\partial w}{\partial x}-\frac{\partial u}{\partial x}\frac{\partial^2 w}{\partial x^2}-\frac{3}{2}\left(\frac{\partial w}{\partial x}\right)^2\frac{\partial^2 w}{\partial x^2}\right]$$
$$-\left[M\frac{\mathrm{d}U_0}{\mathrm{d}t}+(M+m_p)g-\rho_F A_o g\right]\left[\frac{\partial w}{\partial x}-\frac{\partial u}{\partial x}\frac{\partial w}{\partial x}-\frac{1}{2}\left(\frac{\partial w}{\partial x}\right)^3\right]$$
$$-(1-2\mu)(\rho_L A_i-\rho_F A_o)g(L-x)$$
$$\times\left[\frac{\partial^2 w}{\partial x^2}-\frac{\partial^2 u}{\partial x^2}\frac{\partial w}{\partial x}-\frac{\partial u}{\partial x}\frac{\partial^2 w}{\partial x^2}-\frac{3}{2}\left(\frac{\partial w}{\partial x}\right)^2\frac{\partial^2 w}{\partial x^2}\right]$$
$$+(1-2\mu)(\rho_L A_i-\rho_F A_o)g\left[\frac{\partial w}{\partial x}-\frac{\partial u}{\partial x}\frac{\partial w}{\partial x}-\frac{1}{2}\left(\frac{\partial w}{\partial x}\right)^3\right]$$
$$-EA\left[\frac{\partial^2 u}{\partial x^2}\frac{\partial w}{\partial x}+\frac{\partial u}{\partial x}\frac{\partial^2 w}{\partial x^2}+\frac{3}{2}\left(\frac{\partial w}{\partial x}\right)^2\frac{\partial^2 w}{\partial x^2}\right]+EI\frac{\partial^4 w}{\partial x^4}$$
$$-EI\left[3\frac{\partial^3 u}{\partial x^3}\frac{\partial^2 w}{\partial x^2}+4\frac{\partial^2 u}{\partial x^2}\frac{\partial^3 w}{\partial x^3}+2\frac{\partial u}{\partial x}\frac{\partial^4 w}{\partial x^4}+\frac{\partial^4 u}{\partial x^4}\frac{\partial w}{\partial x}\right.$$
$$\left.+2\left(\frac{\partial w}{\partial x}\right)^2\frac{\partial^4 w}{\partial x^4}+8\frac{\partial w}{\partial x}\frac{\partial^2 w}{\partial x^2}\frac{\partial^3 w}{\partial x^3}+2\left(\frac{\partial^2 w}{\partial x^2}\right)^3\right]=0. \tag{13}$$

Under the assumption of the flow velocity in the riser being constant and regardless of the effect of internal and external pressure on cross-section and additional tension, we set the Poisson's ratio μ = 0.5. According to Morison formula, the additional inertial force and fluid

damping force suffered by the riser can be expressed as follows (see Chung et al. 1994*a*)

$$f_w = -C_A\rho_F A_o\dot{V}_{Rw} + \rho_F A_o\dot{V}_{Ww} - \frac{1}{2}C_D\rho_F d_0|V_{Rw}|V_{Rw}, \tag{14}$$

where V_{Rw} is the relative velocity, defined by $V_{Rw} = V_{Pw} + V_{Sw} - V_{Ww}$; $V_{Pw} = \partial w/\partial t$ is the riser velocity in transverse direction, $V_{Sw} = \partial Y/\partial t$ the transverse velocity at any position of the riser induced by the top platform motions and V_{Ww} the wave particle velocity in transverse direction. It should be noted that V_{Rw}, V_{Pw}, V_{Sw}, V_{Ww}, w and Y are functions of x, and Y is the displacement of the riser micro-element due to the surge motion of the top platform. And $\dot{V}_{Rw} = \dot{V}_{Pw} + \dot{V}_{Sw} - \dot{V}_{Ww}$ is the corresponding acceleration in transverse direction, each component of which is acceleration of the riser, top platform and wave particle, respectively. Here f_w denotes the hydrodynamic force applied to the horizontal unit length of the riser, C_A the added mass coefficients, C_D the drag coefficients and d_0 the external diameter of the riser.

Assuming that the riser is simply supported at the both ends, the heave and surge motions of the platform affected by waves can be expressed as

$$\begin{cases} h(t) = h_0 + s_0\cos\omega t \\ y(t) = y_0\sin\omega t \end{cases}, \tag{15}$$

where s_0 and y_0 are amplitudes of platform heave and surge motions respectively, ω denotes the frequency of movement of the platform. According to the corresponding boundary conditions, the solutions of the riser vibration equation can be written as

$$\begin{cases} u(x,t) = h(t)\dfrac{x}{L} + \sum h_l(t)\sin\dfrac{l\pi x}{L} \\ w(x,t) = y(t)\dfrac{x}{L} + \sum f_l(t)\sin\dfrac{l\pi x}{L} \end{cases}, \tag{16}$$

where $l = 0, 1, 2...$

Substituting Eqs. (14) ~ (16) into Eq. (13), and introducing dimensionless quantities

$$\begin{cases} F_n = f_n/d_0, \quad Y_0 = y_0/d_0 \\ S_0 = s_0/d_0, \quad X = x/L \end{cases}, \tag{17}$$

the nonlinear Hill equation describing the parametric excitation of riser can be obtained

$$\frac{\mathrm{d}^2F_n}{\mathrm{d}\tau^2} + \left[\delta^* + \eta^*\varsigma(\tau)\right]F_n + a\int_0^1 P\sin n\pi X\mathrm{d}X + c\int_0^1|Q|Q\sin n\pi X\mathrm{dX}$$
$$= (-1)^{n+1}\frac{8Y_0}{n\pi}\sin 2\tau - \left[1-(-1)^n\right]\frac{16MU_0Y_0}{(M+m_p+m_a)\omega L}\frac{1}{n\pi}\cos 2\tau, \tag{18}$$

where

$$\delta^* = \frac{4}{(M+m_p+m_a)\omega^2}\left\{EA\left[\frac{h_0}{L}\left(\frac{n\pi}{L}\right)^2 + \frac{3}{4}\left(\frac{y_0}{L}\right)^2\left(\frac{n\pi}{L}\right)^2\right]\right.$$
$$\left. - MU_0{}^2\left(\frac{n\pi}{L}\right)^2 + EI\left(\frac{n\pi}{L}\right)^4 - \frac{2EIh_0}{L}\left(\frac{n\pi}{L}\right)^4\right\}, \tag{19}$$

$$\varsigma(\tau) = (\cos 2\tau - K\cos 4\tau + C\cos 2\tau), \tag{20}$$

$$\eta^* = \frac{4EAs_0}{(M+m_p+m_a)\omega^2}\frac{1}{L}\left(\frac{n\pi}{L}\right)^2, \tag{21}$$

$$K = \frac{3}{4}\frac{y_0{}^2}{s_0L}, \tag{22}$$

$$C = \frac{2EI}{EA}\left(\frac{n\pi}{L}\right)^2, \tag{23}$$

$$a = \frac{8MU_0}{(M+m_p+m_a)\omega}, \tag{24}$$

$$c = \frac{C_D\rho_F d_0{}^2}{M+m_p+m_a}, \tag{25}$$

$$P = \sum\frac{l\pi}{L}\frac{\mathrm{d}F_l}{\mathrm{d}\tau}\cos(l\pi X), \tag{26}$$

$$Q = 2Y_0X\cos 2\tau + \sum\frac{\mathrm{d}F_l}{\mathrm{d}\tau}\sin(l\pi X), \tag{27}$$

$$2\tau = \omega t. \tag{28}$$

Here, n, $l = 0,1,2...$ and m_a is the additional water mass.

The Instability Region of Hill Equation

The solutions of Hill's equation will be stable or unstable depending on the combination of parameters δ^*, η^* and K. The unstable solutions will be limited and not grow endlessly in the instability regions, due to the nonlinear damping. The dynamic response amplitudes of the riser in the stability regions are significantly larger than that of instability regions, which will affect the security of riser. According to Eq. (19) and (21), the internal flow density M and internal flow velocity U_0 are items in δ^* and η^*. The existence of internal flow will affect the stability of the parametric excitation of the TTR, and the change of internal flow density and velocity will also affect the stability.

The Hill equation without damping terms can be written as

$$\frac{\partial^2 w}{\partial t^2} + \left[\delta^* + \eta^*\varsigma(t)\right]w = 0. \tag{29}$$

By using Strained Parameter Method, the instability regions boundary of Hill equation can be obtained. We define

$$\begin{cases} w(t,\eta^*) = w_0 + \eta^* w_1 + \eta^{*2}w_2 + \cdots \\ \delta^* = \delta_0^* + \eta^*\delta_1^* + \eta^{*2}\delta_2^* + \cdots \end{cases}, \tag{30}$$

Substituting Eq. (30) into Eq. (29) and expanding by order, solutions of the equation for different orders can be obtained. The zero-order equation can be expressed as

$$w_0 = a\cos nt + b\sin nt, \qquad \text{where } n = 1,2,3... \tag{31}$$

Here, a and b are undetermined coefficients. According to Eq. (31), there is $\delta_0^* = n^2$.

For the purpose of studying the influence of internal flow (including the internal flow density M and internal flow velocity U_0) on the instability regions of the riser, two parameters (δ and η) are introduced here to describe the parametric expression of Hill equation without internal flow. In the present paper, the boundary of the instability regions of Hill equation are deduced using δ, η and internal flow items as variables. The parameter expression of Hill equation without internal flow can be rewritten as

$$\begin{cases} \delta = \dfrac{4}{(m_p+m_a)\omega^2}\left\{EA\left[h_0\dfrac{1}{L}\left(\dfrac{n\pi}{L}\right)^2 + \dfrac{3}{4}\left(\dfrac{y_0}{L}\right)^2\left(\dfrac{n\pi}{L}\right)^2\right]\right. \\ \qquad\qquad \left. + EI\left(\dfrac{n\pi}{L}\right)^4 - 2EIh_0\dfrac{1}{L}\left(\dfrac{n\pi}{L}\right)^4\right\} \\ \eta = \dfrac{4EAs_0}{(m_p+m_a)\omega^2}\dfrac{1}{L}\left(\dfrac{n\pi}{L}\right)^2 \end{cases}, \tag{32}$$

For cases n = 0, 1, 2 and 3, the boundary equation of the instability regions of Hill equation are:

(I) $n = 0$

Using parameters δ^* and η^* for expressing the boundary equation of the instability regions of Hill equation, the boundary equation can be expressed as

$$\delta^* = -\left[\frac{(1-C)^2}{8} + \frac{1}{32}K^2\right]\eta^{*2} + \mathrm{O}(\eta^{*3}). \tag{33}$$

Multiplying both sides of Eq. (33) by δ^*/δ, the boundary equation of the instability regions of Hill equation which uses δ and η to denote can be written as

$$\delta = -\left[\frac{(1-C)^2}{8} + \frac{1}{32}K^2\right]\left(\frac{m_p + m_a}{M + m_p + m_a}\right)\eta^2 + \frac{MU_0{}^2\left(\frac{n\pi}{L}\right)^2}{(m_p + m_a)\omega^2} + \mathrm{O}(\eta^3). \tag{34}$$

The derivations of other cases are similar to Eqs. (33) and (34).

(II) $n = 1$

For case $a = 0$, $\delta_1^* = -K/2$,

$$\delta = \frac{M + m_p + m_a}{m_p + m_a} + \frac{(1-\mathrm{C})\eta}{2} - \frac{m_p + m_a}{m_p + m_a + M}\eta^2 \times\left[\frac{(1-C+K)^2}{32} + \frac{K^2}{96}\right] + \frac{MU_0{}^2\left(\frac{n\pi}{L}\right)^2}{(m_p + m_a)\omega^2} + \mathrm{O}(\eta^3). \tag{35}$$

For case $b = 0$, $\delta_1^* = K/2$,

$$\delta = \frac{M + m_p + m_a}{m_p + m_a} - \frac{m_p + m_a}{M + m_p + m_a}\left[\frac{[K-(1-C)]^2}{32} + \frac{K^2}{96}\right]\eta^2 + \frac{MU_0{}^2\left(\frac{n\pi}{L}\right)^2}{(m_p + m_a)\omega^2} + \frac{(1-C)\eta}{2} + \mathrm{O}(\eta^3). \tag{36}$$

(III) $n = 2$

For case $a = 0$, $\delta_1^* = -K/2$,

$$\delta = \frac{4(M + m_p + m_a)}{m_p + m_a} - \frac{m_p + m_a}{M + m_p + m_a}\eta^2\left[\frac{(1-C)^2}{48} + \frac{K^2}{128}\right] - \frac{K}{2}\eta + \frac{MU_0{}^2(\frac{n\pi}{L})^2}{(m_p + m_a)\omega^2} + \mathrm{O}(\eta^3). \tag{37}$$

For case $b = 0$, $\delta_1^* = K/2$,

$$\delta = \frac{4(M + m_p + m_a)}{m_p + m_a} + \frac{m_p + m_a}{M + m_p + m_a}\eta^2\left[\frac{5(1-C)^2}{48} - \frac{K^2}{128}\right] + \frac{K}{2}\eta + \frac{MU_0{}^2\left(\frac{n\pi}{L}\right)^2}{(m_p + m_a)\omega^2} + \mathrm{O}(\eta^3). \tag{38}$$

(IV) $n = 3$

For case $a = 0$, $\delta_2^* = \frac{(1-C+K)(1-C)}{32} - \frac{(1-C)^2}{64} - \frac{(1-C+K)K}{32} - \frac{K^2}{160}$,

$$\delta = \frac{9(M + m_p + m_a)}{m_p + m_a} + \left(\frac{m_p + m_a}{M + m_p + m_a}\right)\left[-\frac{(1-C)^2}{64} - \frac{(1-C+K)K}{32} + \frac{(1-C+K)(1-C)}{32} - \frac{K^2}{160}\right]\eta^2 + \left(\frac{m_p + m_a}{M + m_p + m_a}\right)^2\left[-\frac{1-C}{1024}K^2 + \frac{1-C+K}{512}(1-C)^2 - \frac{3(1-C)^2}{5120}K + \frac{1-C+K}{1024}K(1-C)\right] + \frac{MU_0{}^2\left(\frac{n\pi}{L}\right)^2}{(m_p + m_a)\omega^2} + \mathrm{O}(\eta^4). \tag{39}$$

For case $b = 0$, $\delta_2^* = \frac{(1-C-K)(1-C)}{32} - \frac{(1-C)^2}{64} - \frac{(1-C-K)K}{32} - \frac{K^2}{160}$,

$$\delta = \frac{9(M + m_p + m_a)}{m_p + m_a} + \left(\frac{m_p + m_a}{M + m_p + m_a}\right)\left[\frac{(1-C-K)(1-C)}{32} - \frac{(1-C)^2}{64} - \frac{(1-C-K)K}{32} - \frac{K^2}{160}\right]\eta^2 + \left(\frac{m_p + m_a}{M + m_p + m_a}\right)^2 \times\left[\frac{1-C-K}{1024}K(1-C) - \frac{1-C-K}{512}(1-C)^2 - \frac{3(1-C)^2}{5120}K + \frac{1-C}{1024}K^2\right]\eta^3 + \frac{MU_0{}^2\left(\frac{n\pi}{L}\right)^2}{(m_p + m_a)\omega^2} + \mathrm{O}(\eta^4). \tag{40}$$

The boundary expressions of the instability regions of Hill equation with internal flow are determined by Eqs. (34) ~ (40). Further, we plot the instability regions of the Hill equation, and the boundary of the instability regions will be some curved surfaces. It needs to be emphasized that the purpose of deriving the instability regions of the Hill equation by using parameters δ and η, which are independent of the internal flow term, is to reflect the effect of the internal flow (internal flow density M and internal flow velocity U_0). If we use the traditional parameters δ^* and η^* to deduce, the instability boundary will be the same as the previous works, and the effect of internal flow terms will not be reflected.

ANALYSIS OF INTERNAL FLOW EFFECTS

Based on the boundary equations of the instability regions of Hill equation established above, the effect of internal flow terms (internal flow density M and internal flow velocity U_0) on instability region is analyzed, and the instability regions of Hill equation under different parameters combination are plotted. The work has concentrated on a 1000 *m* water depth case, and the parameters combination are shown in Table 1.

Effects of Internal Flow Velocity U_0 on Instability Regions

In this section, some cases for different internal flow velocity are used to calculate, where the internal flow volume density is set as ρ_L = 800 kg/m^3. Fig. 3 shows the instability region curved surfaces calculated by Eqs. (34) ~ (40), with the internal flow velocity varying from 0 *m/s* ~ 4 *m/s*. In order to investigate the effect of internal flow velocity U_0 on the instability regions, boundaries of instability region for cases of the internal flow velocity U_0 = 0 *m/s*, 0.5 *m/s*, 1 *m/s*, 2 *m/s*, 3 *m/s* and 4 *m/s* are shown in Fig. 4. Furthermore, the boundaries of the first and second

instability regions under different internal flow velocities ($U_0 = 0$ *m/s*, 2 *m/s* and 4 *m/s*) are shown in Fig. 5. As the internal flow velocity changes, the instability regions are almost the same, as shown in Figs. 4 ~ 5. As we can see from the instability regions boundary Eqs. (34) ~ (40), the internal flow velocity U_0 only exists in the constant term $[MU_0^2(n\pi/L)^2]/[(m_p + m_a)\omega^2]$, which will lead to horizontal translations of the instability regions boundary. For usual liquid flow velocity, the horizontal translations of the instability regions boundary can be negligible because the term $[MU_0^2(n\pi/L)^2]/[(m_p + m_a)\omega^2]$ is small.

Table 1. Parameters combination of TTR.

Parameter Name	Parameter Unit	Parameter value
Length	L (m)	1000
External diameter	d_0 (m)	0.25
Internal diameter	d_i (m)	0.22
Material density	ρ_R (kg/m^3)	7800
Young's modulus	E (Pa)	2.04E11
K	–	0.1875
Platform period	T_P (s)	8
Seawater density	ρ_F (kg/m^3)	1025
Platform amplitude of heave motion	m	0.1
Platform amplitude of surge motion	m	5.0

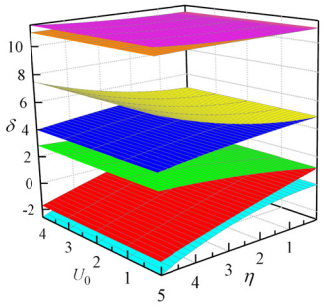

Fig. 3 The 3D surface of the boundaries of instability regions changing with internal flow velocity U_0.

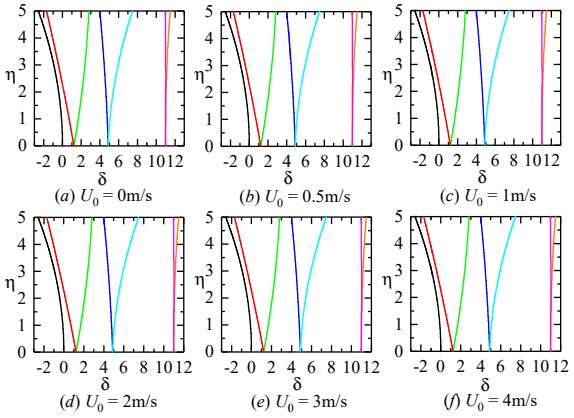

Fig.4 Boundary curves of instability regions for different internal flow velocity. (*a*) $U_0 = 0$ *m/s*; (*b*) $U_0 = 0.5$ *m/s*; (*c*) $U_0 = 1$ *m/s*; (*d*) $U_0 = 2$ *m/s*; (*e*) $U_0 = 3$ *m/s*; (*f*) $U_0 = 4$ *m/s*.

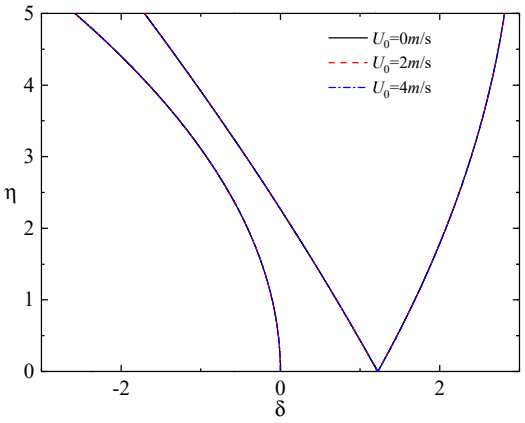

Fig. 5 Boundary curves of the first and second instability regions for different internal flow velocity.

Effects of Internal Flow Density *M* on Instability Regions

In this section, some cases for different internal flow density are used to calculate, where the internal flow velocities are constant ($U_0 = 0$ *m/s* and 1.5*m/s*). Fig. 6 shows the instability region curved surfaces calculated by Eqs. (34) ~ (40) under two internal flow velocities ($U_0 = 0$ *m/s* and 1.5*m/s*), with the internal flow density varying from 0 *kg/m* ~ 40 *kg/m*. For the purpose of studying the effect of internal flow density *M*, boundaries of instability region for cases of the internal flow density $M = 0$ *kg/m*, 15 *kg/m* and 30 *kg/m* for $U_0 = 0$ *m/s* and 1.5*m/s* are shown in Fig. 7 and Fig. 8, respectively. Fig. 7 and Fig. 8 show that, the shape of the instability regions will change, as the internal flow density *M* increases. The boundaries of the first and second instability regions under different internal flow density ($M = 0$ *kg/m*, 15 *kg/m*, and 30 *kg/m*) are shown in Fig. 9. The shape and position of the instability regions will both change with the internal flow density *M*. As we can see from instability regions boundaries Eqs. (34) ~ (40), the internal flow density *M* exists in both constant term $[MU_0^2(n\pi/L)^2]/[(m_p + m_a)\omega^2]$ which is related to the position of the instability regions and the high order terms related to the shape of the instability regions. Therefore, it is understandable that the internal flow density *M* both has effects on the shape and position of the instability regions. But it should be noted that the internal flow density *M* mainly affects the shape due to term $[MU_0^2(n\pi/L)^2]/[(m_p + m_a)\omega^2]$ is small for usual liquid flow velocity.

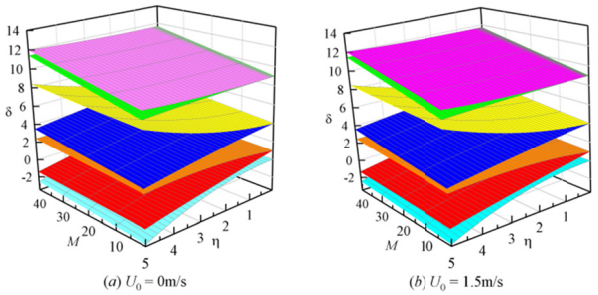

Fig. 6 The 3D surface of the boundaries of instability regions changing with internal flow density *M*. (*a*) $U_0 = 0$ *m/s*; (*b*) $U_0 = 1.5$ *m/s*.

Our calculation also shows that arbitrary points on the boundary of the instability region are shifted by different distances for different internal flow density *M*, which indicates that the internal flow density *M* will both change the shape and position of the instability regions. Here we study the change of points on the δ-axis. We define the distance between two adjacent instability region curves along the δ-axis as

$D^{M}_{n,n+1}$ for a certain internal flow density M (i.e. the distance between the second and the third instability region curves along the δ-axis is $D^{15}_{1,2}$ when internal flow density $M = 15\ kg/m$). When the internal flow

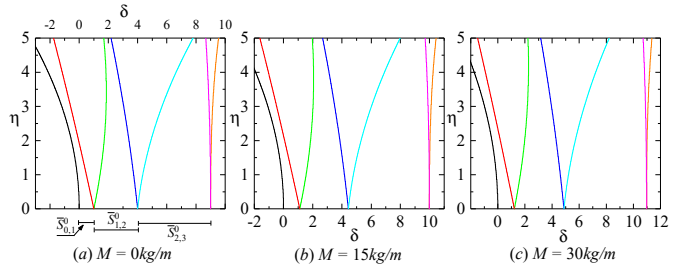

(*a*) $M = 0kg/m$ (*b*) $M = 15kg/m$ (*c*) $M = 30kg/m$

Fig. 7 Boundary curves of instability regions for different internal flow density, where $U_0 = 0\ m/s$.

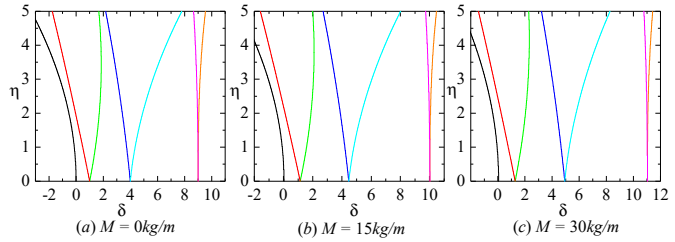

(*a*) $M = 0kg/m$ (*b*) $M = 15kg/m$ (*c*) $M = 30kg/m$

Fig. 8 Boundary curves of instability regions for different internal flow density, where $U_0 = 1.5\ m/s$.

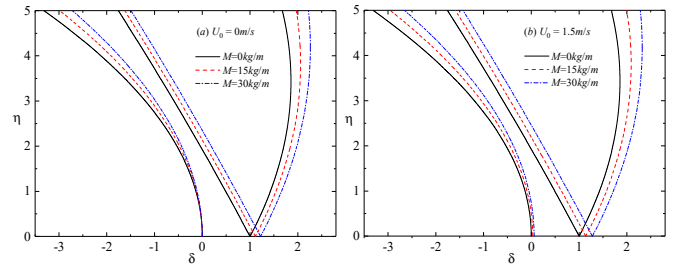

Fig. 9 Boundary curves of the first and second instability regions for different internal flow density. (*a*) $U_0 = 0\ m/s$; (*b*) $U_0 = 1.5\ m/s$.

density $M = 0\ kg/m$, we take the distances, $D^0_{0,1}$, $D^0_{1,2}$ and $D^0_{2,3}$ of the boundary curves of adjacent instability regions along the δ-axis as benchmarks, as shown in Fig. 7(*a*). For a certain internal flow density M, the rate of change of the distance between adjacent instability region boundaries along the δ-axis can be written as

$$\bar{\Delta}^{M}_{n,n+1} = \frac{D^{M}_{n,n+1} - D^{0}_{n,n+1}}{D^{0}_{n,n+1}} \times 100\% . \tag{41}$$

Eq. (41) represents the influences of the internal flow density M on the location of the instability region. Table 2 shows the rate of change of the distances for case $M = 0\ kg/m$, $15\ kg/m$, $20\ kg/m$, $25\ kg/m$ and $35\ kg/m$.

As we can see from Table 2, with the increase of the internal flow density M, the distance between adjacent two instability region boundaries along the δ-axis increases constantly. For a certain internal flow density, rates for distances of different boundaries are nearly equal.

It is found that the change rate of the distance between adjacent instability region boundaries along the δ-axis is linearly related to the internal flow density M. There is

$$\bar{\Delta}^{M}_{n,n+1} = \frac{M}{m_p + m_a} \times 100\% , \qquad \text{for arbitrary } n. \tag{42}$$

Table 2. Rates of change of the distances between adjacent instability region boundaries on the δ-axis for different internal flow densitiy M, where $U_0 = 1.5\ m/s$.

M	$D^{M}_{0,1}$	$\bar{\Delta}^{M}_{0,1}$	$D^{M}_{1,2}$	$\bar{S}^{M}_{1,2}$	$D^{M}_{2,3}$	$\bar{\Delta}^{M}_{2,3}$
0 *kg/m*	1	–	3	–	5	–
15 *kg/m*	1.1102	11.02%	3.3285	10.95%	5.5489	10.98%
20 *kg/m*	1.1468	14.68%	3.4382	14.61%	5.7318	14.64%
25 *kg/m*	1.1834	18.34%	3.5479	18.26%	5.9147	18.29%
35 *kg/m*	1.2565	25.65%	3.7674	25.58%	6.2805	25.61%

With our previous discussion, it can be seen that the internal flow density has influences both on the shape and position of the instability regions. But the effects of the internal flow density on the position of instability regions can be negligible because $[MU_0^2(n\pi/L)^2]/[(m_p + m_a)\omega^2]$ is small for usual liquid flow velocity. As the internal flow density increases, the rate of change of the distance between adjacent instability region boundaries along the δ-axis increases linearly.

CONCLUSIONS

This paper studies the parametric excitation problem of a top-tensioned riser (TTR) with internal fluid subjected to combined platform surge and heave motions. Considering the surge and heave motions of the platform, the internal fluid density and velocity, and the hydrodynamic force on the riser, the nonlinear vibration model of the TTR is established. The nonlinear Hill equation describing the parametric excitation of the TTR and its instability region boundary are obtained. This paper studies the effects of the internal fluid velocity U_0 and the internal fluid density M on instability regions of the Hill equation. The shape of the instability region does not change with the internal fluid velocity U_0 in the riser, and the horizontal translations of the instability regions caused by the internal fluid velocity U_0 can also be negligible for usual liquid flow velocity. In contrast, the shape and position of the instability region of the riser parametric excitation change with the internal flow density M, and the rate of change of the distance between two adjacent instability region boundaries along the δ-axis increases linearly. The relative position of the boundary of two adjacent instability regions is independent of the internal flow velocity U_0.

ACKNOWLEDGEMENTS

This study was supported by the National Natural Science Foundation of China (11672306, 51490673), SKL of HESS (HESS1601), the Strategic Priority Research Program of the Chinese Academy of Sciences (XDB22020100), and the Informatization Plan of the Chinese Academy of Sciences (XXH13506-204).

REFERENCES

Atadan, AS, Calisal, SM, Modi, VJ, and Guo, Y (1997). "Analytical and Numerical Analysis of the Dynamics of a Marine Riser Connected to a Floating Platform," *Ocean Eng*, 24, 111–131.

Brugmans, J (2005). "Parametric Instability of Deep-Water Risers," *Netherlands: Delft University of Technology*.

Chatjigeorgiou, IK (2004). "On the Parametric Excitation of Vertical Elastic Slender Structures and the Effect of Damping in Marine

Applications," *Appl Ocean Res*, 26, 23–33.
Chatjigeorgiou, IK (2010). "On the Effect of Internal Flow on Vibrating Catenary Risers in Three Dimensions," *Eng Struct*, 32, 3313–3329.
Chandrasekaran, S, Chandak, NR, and Anupam, G (2006). "Stability Analysis of TLP Tethers," Ocean Eng, 33, 471–482.
Chatjigeorgiou, IK, and Mavrakos, SA (2002). "Bounded and Unbounded Coupled Transverse Response of Parametrically Excited Vertical Marine Risers and Tensioned Cable Legs for Marine Applications," *Appl Ocean Res*, 24, 341–354.
Chatjigeorgiou, IK, and Mavrakos, A (2005). "Nonlinear Resonances of Parametrically Excited Risers Numerical and Analytical Investigation for $\Omega = 2\omega_1$," *Comput Struct*, 83 (8–9), 560–573.
Chung, JS, and Whitney, AK (1981). "Dynamic Vertical Stretching Oscillation of a Deep–Ocean Mining Pipe," Proc Offshore Tech Conf, Houston, Paper 4092.
Chung, JS, Cheng, BR and Huttelmaier, HP, (1994a). "Three-dimensional coupled responses of a vertical deep-ocean pipe: part I. Excitation at pipe ends and external torsion," *Int J Offshore Polar Eng*, 4(4), 320–330.
Chung, JS, Cheng, BR, and Huttelmaier, HP, (1994b). "Three-dimensional coupled responses of a vertical deep-ocean pipe: part II. Excitation at pipe top and external torsion," *Int J Offshore Polar Eng*, 4(4), 331–339.
Chung, JS (2010). "Full-scale, coupled ship and pipe motions measured in north pacific ocean: the hughes glomar explorer with a 5,000-m-long heavy-lift pipe deployed," *Int J Offshore Polar Eng*, 20(1), 1–6.
Fujiwara, T, Uto, S, and Kanada, S (2011). "An Experimental Study of the Effects that Change the Vibration Mode of Riser VIV," *In: Proceedings of the ASME 30th International Conference on Ocean, Offshore and Artic Engineering*, Rotterdam, Netherlands, OMAE2011–49677, 487–492.
Guo, HY, and Lou, M (2008). "Effect of Internal Flow on Vortex-Induced Vibration of Risers," *J Fluid Struct*, 24, 496–504.
Hsu, CS (1975). "The Response of a Parametrically Excited Hanging String in Fluid," *J Sound Vib*, 39, 305–316.
Kuiper, GL, Brugmans, J, and Metrikine, AV (2008). "Destabilization of Deep-Water Risers by a Heaving Platform," *J Sound Vib*, 310, 541–557.
Keber, M, and Wiercigroch, M (2008). "Dynamics of a Vertical Riser with Weak Structural Nonlinearity Excited by Wakes," *J Sound Vib*, 315, 685–699.
Lei, S, Zhang, WS, Lin, JH, Yue, QJ, Kennedy, D, and Williams, F (2014). "Frequency Domain Response of a Parametrically Excited Riser under Random Wave Forces," *J Sound Vib*, 333, 485–498.
Lei, S, Zheng, XY, and Chen, DY (2017). "Instability Analysis of Parametrically Excited Marine Risers by Extended Precise Integration Method," *Int J Struct Stab Dyn*, 17(8), 1750096.
Li, LX, and Chen, LY (2018). "Parametric Instability Analysis of the Top-Tensioned Riser in Consideration of Complex Pre-stress Distribution," *Adv Mech Eng*, 10(1), 1–11.
Meng, D, and Chen, L (2012). "Nonlinear Free Vibrations and Vortex-Induced Vibration of Fluid Conveying Steel Catenary Riser," *Appl Ocean Res*, 34, 52–67.
Meng, S, Kajiwara, H, and Zhang, WJ (2017a). "Internal Flow Effect on the Cross-flow Vortex Induced Vibration of a Cantilevered Pipe Discharging Fluid," *Ocean Eng*, 137, 120–128.
Meng, S, Song, SD, Che, CD, and Zhang, WJ (2018). "Internal Flow Effect on the Parametric Instability of Deepwater Drilling Risers," *Ocean Eng*, 149, 305–312.
Meng, S, Zhang, XQ, Che, CD,and Zhang, WJ (2017b). "Cross-Flow Vortex-Induced Vibration of a Flexible Riser Transporting Flow from Subcritical to Supercritical," *Ocean Eng*, 139, 74–84.
Paidoussis, MP (1998). "Fluid-Structure Snteractions: Slender Structures and Axial Flow," *Academic press*.
Park, H, and Jung, DH (2002). "A Finite Element Method for Dynamic Analysis of Long Slender Marine Structures under Combined Parametric and Forcing Excitations," *Ocean Eng*, 29, 1313–1325.
Patel, MH, and Park, HI (1995). "Combined Axial and Lateral Responses of Tensioned Buoyant Platform Tethers," *Eng Struct*, 17,687–695.
Wang, Y, Gao, D, and Fang, J (2015). "Coupled Dynamic Analysis of Deep-water Drilling Riser under Combined Forcing and Parametric Excitation," *J Nat Gas Sci Eng*, 27(3), 1739–1747.
Wu, MC, and Lou, JYK (1991). "Effects of Rigidity and Internal Flow on Marine Riser Dynamics," *Appl Ocean Res*,13, 235–244.
Xu, WH, Zeng, XH, Wu, YX, and Liu, JY (2008). "Hill Instability Analysis of TLP Tether Subjected to Combined Platform Surge and Heave Motions," *China Ocean Eng*, 22(4), 533–546.
Xu, WH, Wu, Y X, Zhong, XF, He, Y, Liu, PL, and Feng, XH (2011). "Methods for Parametric Excitation Instability Analysis of Slender Flexible Cylindrical Structures in Offshore Engineering," *J Shock Vib*, 30(9),79–83.
Yang, H, Xiao, F, and Xu, P (2013). "Parametric Instability Prediction in a Top-Tensioned Riser in Irregular Waves," *Ocean Eng*, 70, 39-50.
Zhang, J, and Tang, Y (2015). "Parametric Instability Analysis of Deepwater Top-Tensioned Risers Considering Variable Tension along the Length," *J Ocean Univ China*, 14(1), 59–64.